CIRCLE PACKING WITH GENERALIZED BRANCHING

JAMES ASHE, EDWARD CRANE AND KENNETH STEPHENSON

Dedicated to C. David Minda on the occasion of his retirement

Classical analytic function theory is at the heart of David Minda's research and of many of the results in this volume. It has been a pleasure in recent years to discover that simple patterns of circles called circle packings could find themselves in such tight company with this classical theory. David himself contributed to this topic in [10] and on his retirement will surely have time to dive back into it.

Let us briefly review the circle packing story line. In 1936 Koebe showed in [**?**] that for every abstract triangulation K of a topological sphere there exists an essentially unique configuration of circles with mutually disjoint interiors on the Riemann sphere $\mathbb{P}$ whose pattern of tangencies is encoded in K. That is, there is a circle packing P for K in $\mathbb{P}$. This fact was rediscovered in the 1970s by Andreev [1, 2] as a special case of a classification of hyperbolic polyhedra in terms of their dihedral angles, (see also [**?**] for a correction and commentary). It was noticed again by Bill Thurston in the 1980s. Inspired by the rigidity of circle packings, Thurston made a remarkable proposal at the 1985 Conference in Celebration of de Branges' Proof of the Bieberbach Conjecture, that one could use such circle packings to approximate conformal mappings. The subsequent proof of Thurston's conjecture by Burt Rodin and Dennis Sullivan [11] established circle packing as a topic in its own right and opened its most widely known aspect, the approximation of classical analytic functions.

As this approximation theory developed, a second aspect that we will call *discrete analytic function theory*, began to emerge. For it became increasingly clear that classical phenomena were already at play within circle packing — mappings between circle packings not only approximated analytic functions, they also mimicked them. The literature shows an ever growing list of conformal notions being realized discretely and often with remarkable geometric fidelity. Moving circle packing into the hyperbolic geometry of $\mathbb{D}$ led to infinite packings and the consequent classical type conditions — the spherical, hyperbolic, and euclidean trichotomy. Then came the discrete uniformization theorem, discrete Riemann surfaces and covering theory, connections with random walks, and notions of branch points and boundary conditions. Discrete analogs of familiar classes of functions

Date: November 8, 2016.

were developed: polynomials, exponentials, and the Blaschke products and Ahlfors functions that play their roles in this paper.

Part and parcel in these developments has been a third aspect, computation. Circle packings demand to be seen; that has led to packing algorithms, followed by experiments, then new — often surprising — observations, augmented theory, more computations, on and on. The work here was motivated by computational challenges, and the images behind our work are produced with the open software package `CirclePack`, [13].

Step after step in this story one can observe the remarkable faithfulness of the discrete theory to its continuous precedents so that today one can claim a fairly comprehensive discrete world parallel to the classical world of analytic functions (and invariably converging to it in the limit as the combinatorics are refined). Yet this discrete world can never be fully comprehensive, one always faces "discretization issues". This paper is a preliminary description of new machinery for addressing the principal remaining gap in the foundation of discrete function theory, the existence and uniqueness of discrete meromorphic functions. The sphere is a difficult setting for circle packing. On the practical side, there is no known algorithm for computing circle packings *in situ*, restricting the experimental approach; essentially all circle packings on $\mathbb{P}$ have been obtained *via* the stereographic projection of hyperbolic or euclidean packings. More crucially, the compactness of the sphere brings conformal rigidity, with topologically mandated branching and no boundary to provide maneuvering room.

Difficulties caused by the rigidity of branching locations are the discretization issue we address here. We introduce generalized branching, which began with the thesis of the first author, [3]. We believe general branching will provide the flexibility necessary to construct the full spectrum of discrete branched mappings while keeping two main objectives at the fore: (1) discrete analytic functions should display qualitative behaviors parallel to their classical counterparts, and (2) discrete analytic functions should converge under refinement to their classical counterparts.

1. Classical Models

We use two types of classical functions to motivate this work: finite Blaschke products on the unit disc and Ahlfors functions on annuli. We review these in preparation for their discrete versions.

Blaschke Products: A classical finite Blaschke product $\mathbf{B} : \mathbb{D} \to \mathbb{D}$ is a proper analytic self map of the unit disc $\mathbb{D}$. In particular, $\mathbf{B}$ has finite valence $N \geq 1$, it maps the unit circle N times around itself, and it has $N-1$ branch points in $\mathbb{D}$, counting multiplicities — that is $\mathbf{B}'$ has $N-1$ zeros in $\mathbb{D}$. The function $\mathbf{B}$ is known as an N-fold Blaschke product. Topologically

speaking, $\mathbf{B}$ maps $\mathbb{D}$ onto an N-sheeted complete branched covering of $\mathbb{D}$. The images of the branch *points* under $\mathbf{B}$ are known as branch *values*.

As a concrete example, let us distinguish two points $p_1 \neq p_2$ in $\mathbb{D}$. It is well known that there exists a 3-fold Blaschke product $\mathbf{B}$ with p_1, p_2 as simple branch points. It is convenient to assume a standard normalization, so by post-composing with a conformal automorphism (Möbius transformation) of $\mathbb{D}$ we may arrange further that $\mathbf{B}(0) = 0$ and $\mathbf{B}(i) = i$. This is the function we will have in mind for discretization later.

Ahlfors Functions: Our next model is defined on a proper annulus Ω. By standard conformal mapping arguments, we may take Ω to be a *standard* annulus, $\Omega = \{z : r < |z| < 1/r\}$, with $0 < r < \infty$. Designating a point $z_0 \in \Omega$, one may consider the extremal problem: maximize $|\mathbf{F}'(z_0)|$ over all analytic functions $\mathbf{F} : \Omega \to \mathbb{D}$. The solution $\mathbf{A}(z)$ is known to exist, is unique up to multiplication by a unimodular constant, and is referred to as an *Ahlfors* function for Ω. Ahlfors functions are also characterized, however, by their mapping properties. They are the proper analytic mappings $\mathbf{A} : \Omega \to \mathbb{D}$ which extend continuously to $\partial\Omega$ and map each component of $\partial\Omega$ 1-to-1 onto the unit circle. Any such map will be a branched double covering of $\mathbb{D}$ with two simple branch points, $p_1, p_2 \in \Omega$. It is fundamental to function theory on Ω and is analogous to the 1-fold Blaschke products on $\mathbb{D}$, i.e., Möbius transformations. The Ahlfors function for Ω is determined uniquely by r (up to pre- and post-composition by conformal automorphisms).

To have a concrete example in mind for discretization, let us suppose that z_0 is on the midline of Ω, say $z_0 = 1$. From elementary symmetry considerations we deduce that $\mathbf{A}(1) = \mathbf{A}(-1) = 0$ and that the branch points in Ω lie at $p_1 = i$ and $p_2 = -i$. A normalization in the range, $\mathbb{D}$, will put the branch values on the imaginary axis, symmetric with respect to the origin.

Note that while both classes of functions are characterized by their topological mapping properties, only with the Blaschke products do we get any choice in the branch points — for Ahlfors functions, the branch point locations are (up to normalization) forced on us by the conformal geometry of the domain.

2. Discrete Versions

We will now describe and illustrate discrete versions of these classical functions. We assume a basic familiarity with circle packing, as presented in [14] for example. However, a brief overview might help, and with the images here should aid the intuition, even for those not familiar with details.

A *discrete analytic function* is a map between circle packings. The domain, rather than being a Riemann surface, will now be a triangulated topological surface with combinatorics encoded as a simplicial 2-complex K: thus, we will be selecting K to be a combinatorial disc or a combinatorial annulus, as appropriate. A *circle packing* for K is a configuration P of oriented circles (or discs), $P = \{c_v\}$ with a circle c_v associated with each vertex v of K. The circle packing may live in the euclidean plane, $\mathbb{C}$, in the hyperbolic plane, represented as the unit disc $\mathbb{D}$, or on the Riemann sphere, $\mathbb{P}$. In the hyperbolic plane we allow horocycles in place of circles to represent vertices on the boundary of K, taking the 'center' of the horocycle to be its basepoint in the ideal boundary; in the Poincaré model this is the point of tangency with the unit circle. The only requirements for a packing are that whenever $\langle v, w\rangle$ is an edge of K, then circles c_v, c_w must be (externally) tangent, and when $\langle u, v, w\rangle$, is an oriented face of K, then the circles c_u, c_v, c_w must form an oriented triple of mutually tangent circles. There is no requirement that the interiors of the discs be mutually disjoint; if they are then we say the packing is *univalent*. The *carrier* of P, denoted $\mathrm{carr}(P)$, is the polyhedral surface obtained by equipping each face $\langle u, v, w\rangle$ of K with the geometry of the geodesic triangle joining the centers of the circles c_u, c_v, c_w. That is, $\mathrm{carr}(P)$ is a realization of the abstract triangulation K as a concrete oriented triangulated surface equipped with a metric and a map to the ambient space $\mathbb{C}$, $\mathbb{D}$ or $\mathbb{P}$. When the packing is univalent, we can think of the carrier as embedded in the ambient space. A packing can be locally univalent, meaning that the star of each vertex in $\mathrm{carr}(P)$ is embedded in the ambient space, without being globally univalent; then the map to the ambient space is an immersion. A packing that is not locally univalent is called a *branched* circle packing.

At the foundation of the theory is the fact that each complex K has a canonical *maximal packing* $P_K = \{C_v : v \in K\}$. This is a univalent circle packing, meaning the circles have mutually disjoint interiors, which fills $\mathbb{D}$ or a conformal annulus, as the case may be. The packing P_K serves as the domain for discrete analytic functions associated with K. The image will be a second circle packing P for K which lies in $\mathbb{D}$. The discrete analytic function, then, will be the map $\mathbf{f} : P_K \to P$ which identifies corresponding circles. (One may also treat $\mathbf{f}$ as a piecewise affine mapping $\mathbf{f} : \mathrm{carr}(P_K) \to \mathrm{carr}(P)$ by mapping circle centers to circle centers and extending *via* barycentric coordinates to edges and faces.)

We are now ready for the discrete constructions. Central to our work is the issue of branching, as we will see in this first discrete example.

2.1. **Discrete Blaschke Product.** In a sense, discrete function theory began with the introduction of discrete Blaschke products; see [9] and [14,

§13.3]. The construction here will serve to remind the reader of basic notation and terminology while providing an example directly pertinent to our work.

A discrete finite Blaschke product $\mathbf{b}$ is illustrated in Figure 1, with the domain circle packing P_K on the left and the image circle packing P on the right, both in $\mathbb{D}$. There is nothing special in the underlying complex K, a combinatorial disc — it is just a generic triangulation of a topological disc, though there are minor combinatorial side conditions to avoid pathologies once we impose branching.

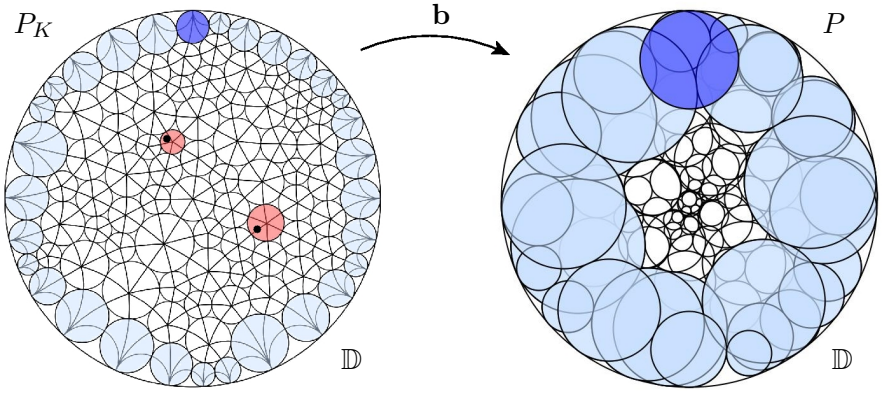

FIGURE 1. A 3-fold discrete Blaschke product $\mathbf{b}$, domain and range.

Begin with the domain packing for $\mathbf{b}$ on the left, the maximal packing $P_K = \{C_v : v \in K\}$. The boundary circles are horocycles (euclidean circles internally tangent to $\partial\mathbb{D}$). A designated interior vertex α has its circle C_α centered at the origin and a designated boundary vertex γ has its 'circle' (actually a horocycle) C_γ 'centered' at $z = i$, the basepoint of the horocycle on the ideal boundary of the Poincaré model. The horocycle representing γ appears here as dark blue. The classical Blaschke product $\mathbf{B}$ discussed earlier involved branch points p_1, p_2; we assume these are the two black dots in the domain. To mimic this, we have identified interior circles C_{v_1}, C_{v_2}, red circles, whose centers are nearest to p_1, p_2, respectively.

Note that the unit disc is treated as the Poincaré model of the hyperbolic plane, so circle centers and radii are hyperbolic and the carrier faces are hyperbolic triangles. The boundary circles, as horocyles, are of infinite hyperbolic radius and have hyperbolic (ideal) centers at their points of tangency with the unit circle. The set of hyperbolic radii is denoted by $R_K = \{R_K(v)\}$. The existence of P_K follows from the fundamental Koebe-Andreev-Thurston Theorem, [14, Chp 6], as does its essential uniqueness up to conformal automorphisms of $\mathbb{D}$. In practice, however, it is computed

based on angle sum conditions. The *angle sum* $\theta_{R_K}(v)$ at a vertex v is the sum of angles at v in all the faces to which it belongs and is easily computed from the radii R_K using basic hyperbolic trigonometry. Clearly, one must have $\theta_{R_K}(v) = 2\pi$ for every interior v. This, along with the condition that $R_K(w) = \infty$ for boundary vertices w, is enough to solve for R_K. There are several numerical methods available for computing R_K. One method is to use a variational principle, finding the minimum of a carefully chosen convex function of (functions of) the radii, whose critical point corresponds to the solution. This idea was first introduced by Y. Colin de Verdière [**?**], and a number of such functionals for the hyperbolic case are described in [**?**]. Alternatively one can use an iterative method based on the upper Perron method of [5], computing a pointwise decreasing sequence of approximations to R_K. We give some more details of this below in §5. Faster methods exist and are implemented in `CirclePack` see for example [7].

Let us now move to the more visually challenging range packing in Figure 1, denoted $P = \{c_v : v \in K\}$. This, too, is a hyperbolic circle packing for K, though it is clearly not univalent. We have arranged that the circle c_α is centered at the origin and that the circle c_γ is a horocycle centered at $z = i$, just as in P_K. The boundary circles are again horocycles, and if one starts at c_γ and follows the counterclockwise chain of successively tangent horocycles, one finds that they wraps three times about the unit circle. This mimics the behavior of our 3-fold classical Blaschke product $\mathbf{B}$.

The image of P is a bit too fussy to show its carrier, but it is in fact a 3-sheeted branched surface. Hidden among the interior circles of P are the two associated with vertices v_1, v_2, the branch vertices. These circles, red in both domain and range, are difficult to pick out, but since branching is the central topic of the paper, we have blown up the local images at v_1 in Figure 2. We now describe what you are seeing.

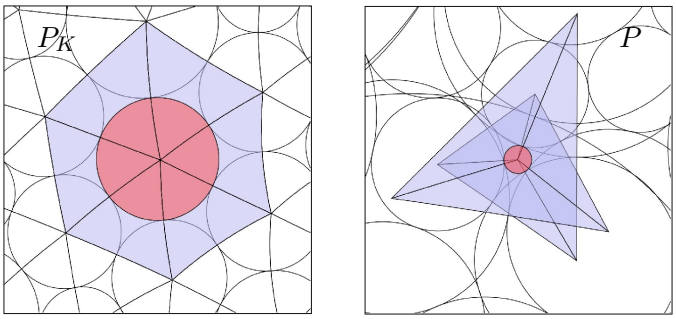

FIGURE 2. Isolated flowers for the branch vertex v_1 in the domain P_K and range P of the discrete Blaschke product $\mathbf{b}$.

This branching will be termed *traditional*; conceptually and computationally very simple, this mechanism for achieving branching in a circle packing

has, until now, provided all the branching for discrete function theory, [14, §11.3]. The flower for vertex v, the central circle (red) and its neighboring circles (its *petals*), are shown for P_K on the left and for P on the right. Whereas the six petals wrap once about C_{v_1} in the domain, a careful check will show that they wrap twice around c_{v_1} in the range. If R denotes the set of hyperbolic radii for P, we may compute the angle sum $\theta_R(v_1)$ at c_{v_1}. Expressed in terms of angle sums, the branching is reflected in the fact that $\theta_{R_K}(v_1) = 2\pi$ in the domain, while $\theta_R(v_1) = 4\pi$ in the range. Mapping the faces about C_{v_1} onto the corresponding faces about c_{v_1} realizes a 2-fold branched cover in a neighborhood of the center of c_{v_1} — meaning a branched covering surface in the standard topological sense. Similar behavior could be observed locally at the other branch vertex, v_2, while at all other interior vertices the map between faces is locally univalent.

In summary, the circle packing map $\mathbf{b} : P_K \to P$ is called a *discrete finite Blaschke product* because it displays the salient mapping features of the classical Blaschke product $\mathbf{B}$: namely, $\mathbf{b}$ is a self-map of $\mathbb{D}$, a 3-fold branched covering, it maps the unit circle 3 times about itself, and it harbors two interior branch points. We have even imposed the same normalization, $\mathbf{b}(0) = 0$ and $\mathbf{b}(i) = i$.

Existence and uniqueness theorems for discrete finite Blaschke products of arbitrary degree, and additional features of such discrete analytic functions were developed in [5, 6, 9]. The combinatorial side condition mentioned above says that in order for the branched packing to exist, there must be no simple closed cycle of fewer than $2n + 3$ edges in the complex that winds around any n branch points, counted with multiplicity.

Note in Figure 2 how much the circles for a branch vertex shrink under $\mathbf{b}$; this ratio of radii mimics the vanishing of the derivative at a branch point. Note in Figure 1 how $\mathbf{b}$ draws the interior circles together; this is the discrete hyperbolic contraction principle. Note that the circles for α are centered at the origin in both P_K and P, but the latter is much smaller: this reflects the discrete Schwarz Lemma. On the other hand, the horocycle associated with γ (blue) is much larger in P than in P_K, reflecting the behavior of angular derivatives at the boundary. Discrete analytic function theory is rife with such parallel phenomena for a wide variety of situations, including the Ahlfors example that we treat next.

2.2. **Discrete Ahlfors Function.** We build a clean example that mimics the classical Ahlfors function $\mathbf{A}$ described earlier. Our complex K triangulates a topological annulus. Its maximal packing P_K is represented in Figure 3.

A bit of explanation may help here: The maximal packing actually lives on a conformal annulus $\mathcal{A}$, with circles measured in its intrinsic hyperbolic metric. However, as $\mathbb{D}$ is the universal cover of $\mathcal{A}$, we can lift the packing

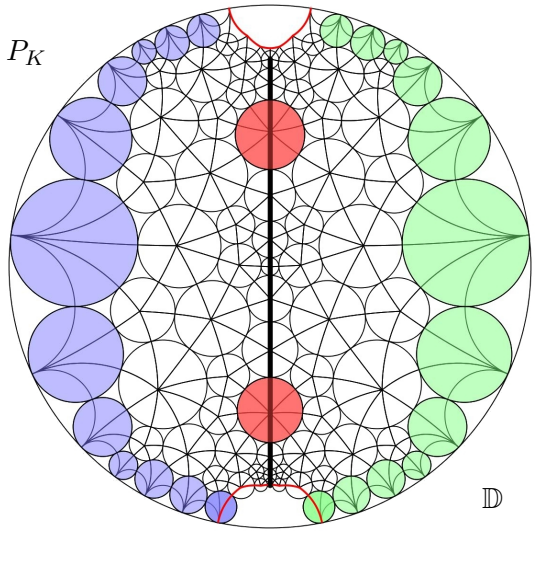

a

FIGURE 3. Maximal packing P_K for a combinatorial annulus K, represented in a fundamental domain in $\mathbb{D}$.

to lie in a fundamental domain within $\mathbb{D}$ — that is what we see in Figure 3. The boundary edges in red represent the lifts of a cross-cut of $\mathcal{A}$ and are identified by the hyperbolic Möbius transformation γ of $\mathbb{D}$ which generates the covering group for $\mathcal{A}$. Applying γ to the circles of Figure 3, one would get new circles which blend seamlessly along the cross-cut.

We have chosen K with foresight, as it displays two particularly helpful symmetries. The line in the center of Figure 3 marks the combinatorial midline of the annulus: K is symmetric under reflection in this. Moreover, there is an order two translational symmetry along this midline, by the hyperbolic Möbius transformation $\sqrt{\gamma}$ whose square is γ. This carries P_K to itself, modulo the group generated by γ. Topology demands, as with the classical Ahlfors function $\mathbf{A}(z)$, that we have two simple branch points. Choose the midline vertices v_1 and v_2, their circles are red in Figure 3; these two are fixed by the reflective symmetry and interchanged by the translational symmetry. Prescribing traditional branching at v_1, v_2 results in the branched circle packing, P, of Figure 4. The mapping $\mathbf{a} : P_K \to P$ is thus a discrete analytic function from $\mathcal{A}$ to $\mathbb{D}$.

Due to its mapping properties, we refer to $\mathbf{a}$ as a *discrete Ahlfors function*. In particular: The boundary circles of P_K are horocycles; in Figure 3, those on one boundary component are blue, those of the other, green. We would expect the boundary circles of P to be horocycles as well, meaning that $\mathbf{a}$ maps each boundary component to the unit circle. With a careful look in Figure 4, one can disentangle the closed chain of blue horocycles reaching

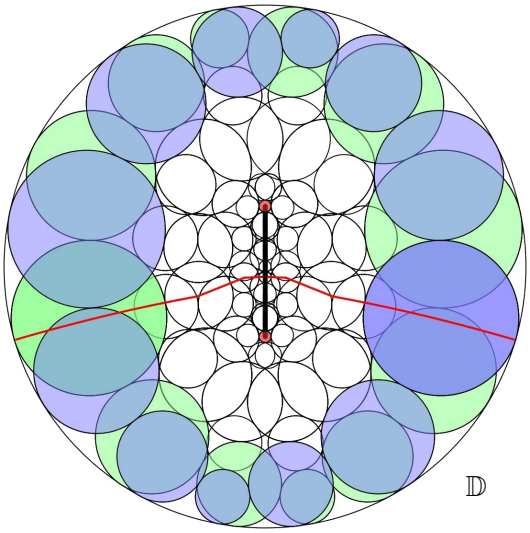

FIGURE 4. The branched packing P for combinatorial annulus K.

once around the unit circle and the second closed chain of green horocycles doing the same. The branch circles, C_{v_1}, C_{v_2} in P_K, and their images, c_{v_1}, c_{v_2} in P, are red. We have normalized by applying an automorphism to $\mathbb{D}$ that centers c_{v_1} and c_{v_2} on the imaginary axis and symmetric with respect to the origin. Thus, P represents in a discrete way a double covering of $\mathbb{D}$ branched over two points. These are all hallmarks of the image of an Ahlfors function and mimic the classical function $\mathbf{A}$. For reference, in P we have drawn in red the edges of P corresponding to red cross-cut in P_K.

The computation of P deserves special attention. The upper Perron method of Bowers [5] allows one to compute a hyperbolic packing label R for K so that $R(w) = \infty$ for each boundary vertex $w \in K$ and angle sums $\theta_{R_K}(v_j) = 4\pi$ for v_1, v_2. There is nothing special in computing R. There is a second step, however: with R in hand, one then lays out the circles. This means that one chooses tangent positions for the circles representing vertex α and a neighbor vertex β and then computes the locations in $\mathbb{D}$ of all the other circles in turn, to satisfy the tangency and orientation conditions: whenever there is a face of K for which the location of the circles representing two of the vertices is known then the location of the third can be deduced. Finally one applies a normalizing Möbius transformation to get the packing P of Figure 4. But *why* does this second step work so nicely? In circle packing, the laying out of circles is akin to analytic continuation of an analytic function element, and since K is an annulus, its fundamental group is generated by some simple, closed, nonnullhomotopic loop Γ. Analytic continuation along Γ would generically lead to a non-trivial holonomy:

that is, given a function element $\mathfrak{f}$ defined at a point of Γ, one would anticipate a non-trivial automorphism m of $\mathbb{D}$ so that analytic continuation of $\mathfrak{f}$ about Γ would lead to a new element $m(\mathfrak{f})$, $m(\mathfrak{f}) \neq \mathfrak{f}$. In discrete terms, after laying out the circle c_v for some vertex v of Γ, and then laying out successively tangent circles for the vertices along Γ, one would not expect that upon returning to v one would lay out the same circle c_v. Generically, there is a non-trivial automorphism m so that upon returning to v one lays out $m(c_v) \neq c_v$. As it happens here, things work out because of the symmetries built into K — we will prove that these symmetries force the holonomy m to be trivial, so the layout process results in a coherent branched circle packing P. In fact the translational symmetry of K is represented under the holonomy by an element $g \in \mathrm{Aut}(\mathbb{D})$ such that $g^2 = m$. The reflection symmetry of K is represented by an orientation-reversing isometry h of $\mathbb{D}$, which has a hyperbolic geodesic of fixed points; we can take to be the imaginary axis, as illustrated in Figure 4. Since g and h commute, g fixes the imaginary axis setwise. The branch vertex v_1 is fixed by the reflection so its circle is centred on the imaginary axis. The simple branching at v_1 then forces g to reverse the orientation of the imaginary axis. Hence g is an elliptic involution and m is the identity. In Figure 4 the fixed point of g is at 0. The holonomy issue is key to later considerations.

The good news is that we have successfully created discrete analogues for our two classical models: Blaschke products and Ahlfors functions. Let us now look into the bad news.

3. The Discretization Issue

Whenever a continuous theory is discretized, whether in geometry, topology, differential equations, or p-adic analysis, problems will crop up. Replacing a continuous surface by a triangulated one, for example, leads to combinatorial restrictions. For example a simple branch vertex must be an interior vertex and must have at least 5 neighbors: it is simply not possible for four or fewer circles to form a closed chain of petals wrapping twice around another circle. Likewise a double branch vertex must have at least 7 neighbors for the petals to be able to wrap around three times, and so on. However, there is another important discretization effect: *there are only finitely many possible locations for discrete branching*. Our discrete Blaschke product could not branch precisely at the points p_1, p_2 prescribed for its classical model $\mathbf{B}$, and we instead chose to branch using the nearby circles C_{v_1} and C_{v_2}. This effect is admittedly minor — the qualitative behavior of the discrete function is little affected by the misplaced branching. For the Ahlfors function, however, this problem is existential — discrete versions may fail to exist. We will illustrate the problem in the Ahlfors cases — and return to fix it in §6.

Nearly any break in the combinatorial symmetries of the complex K behind Figure 3 will cause the subsequent Ahlfors construction to fail. Most such failures will be difficult to fix, so we choose carefully: we make two small changes *via* edge flips so that we preserve the reflective symmetry but break the translational symmetry. The new complex will be denoted K'. Repeating the Ahlfors construction from §2.2 with K' and using the same v_1, v_2 as branch vertices gives the result of Figure 5.

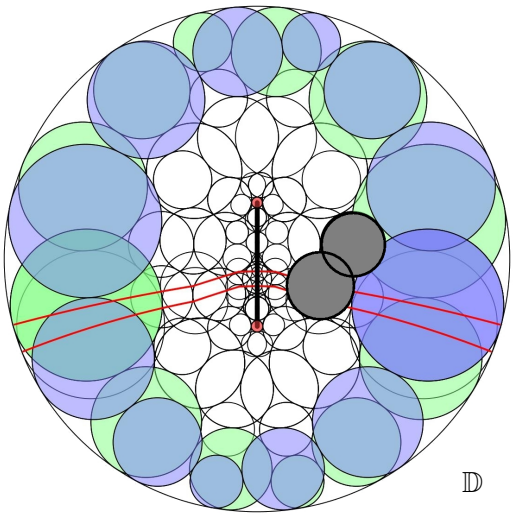

FIGURE 5. A failed attempt at an Ahlfors function using traditional branching. The non-trivial holonomy shows up in misalignment of the cross-cuts, and the failure of the gray circles to be tangent to one another.

There is no difficulty in computing the branched packing label R' for K', however, the layout process does not give a coherent circle packing. The problem might be difficult to see in Figure 5, but look at the red edge paths, which correspond to layouts of the cross-cut: they are no longer coincident, as they were in Figure 4. One is a shifted copy of the other, reflecting a non-trivial holonomy associated with the generator of the fundamental group for K'. More precisely, there is a non-trivial hyperbolic Möbius transformation m of $\mathbb{D}$, which maps one of these red cross-cut curves onto the other. One would have to follow things very closely in the image to confirm the problem, but we illustrate with the two gray circles, which are supposed to be tangent to one another.

As it happens, no matter what pair of vertices of K' are chosen as branch points, the Ahlfors construction will fail — there will be no coherent image packing. It has been a long road to get to this point, but this is where our work begins: Our goal is to introduce *generalized* branching with the

flexibility to make the discrete theory whole. We will illustrate it in action in §6 by creating an Ahlfors function for this modified complex K'.

4. Generalized Branching

Branching is perhaps most familiar in the analytic setting. Let $\mathbf{f} : G \to \mathbb{C}$ be a non-constant analytic function on an open domain $G \subset \mathbb{C}$. Suppose $z \in G$ and $w = \mathbf{f}(z)$. For $\delta > 0$, consider the disc $D = D(w, \delta) = \{\zeta : |\zeta - w| < \delta\}$ and the component of the preimage $U = \mathbf{f}^{-1}(D(w, \delta))$ containing z. For δ sufficiently small, U will be a topological disc in G and the restriction of $\mathbf{f}$ to the punctured disc $U' = U \backslash \{z\}$ will be a locally 1-to-1 proper mapping onto the punctured disc $D' = D \backslash \{w\}$. In particular, one can prove the existence of some $N \geq 1$ so that every point of D' has N preimages in U'. In this analytic case, if $N > 1$, then $\mathbf{f}^{(k)}(z) = 0$ for $k = 1, 2, \cdots, N-1$ and we say that z is a *branch point* of order $N - 1$ for $\mathbf{f}$. We refer to w as its *branch value*.

This is, in fact, a topological phenomenon having little to do with analyticity: by Stoïlow's Theorem, [**?**, Thm 5.1, p. 198], the same local behavior occurs whenever the map $\mathbf{f}$ is an open, continuous, and light mapping. In particular, this applies to the piecewise affine map from the carrier surface of a branched circle packing to the ambient space of the packing. One sees it on display for the traditional branch point illustrated in Figure 2.

We now change our viewpoint slightly, and think of a branched circle packing as a packing of discs on a branched covering surface S of a domain U in the Riemann sphere, complex plane or unit disc. Although their projections to U overlap, these discs must have disjoint interiors when thought of as subsets of S. The discs are closed balls in the metric obtained by lifting the Riemannian metric (spherical, Euclidean or hyperbolic) to the covering surface. This *pullback metric* on the covering surface fails to be a Riemannian metric with respect to the natural smooth structure on the covering surface, because it has conical singularities at the branch points each with total angle in the set $\{4\pi, 6\pi, 8\pi \ldots\}$. Nevertheless, if a closed ball in S does not contain a branch point in its interior then projects one-to-one onto a disc in U. A closed ball in S whose center is a branch point projects as a proper branched covering of a disc in U, as long as it contains no other branch point. Thus we have an interpretation of both unbranched circles and traditional branch circles as discs in S.

What else can happen? It is not possible for a branch point p to lie in a non-empty open interstice between three mutually tangent discs on S, because each disc subtends an angle less than π at p and the total angle around p on S is at least 4π. However, it is possible for three or more unbranched circles to meet at a branch point on S, yet still have disjoint interiors. In fact, at a branch point of multiplicity k, where $k+1$ sheets of S

meet, up to $2k+2$ circles can fit together with disjoint interiors. If only three discs meet at a simple branch point ($k = 1$) then there is some flexibility in the configuration, and we will later parameterize this. We call the situation where three or more discs meet at a branch point *singular branching*.

We have also opened up the possibility of using a closed metric ball on S that contains a branch point z in its interior but not at its center, x. Under the projection to U, the image of the boundary of such a ball is a pair of circles: a large circle centered at the projection of x and a smaller circle that is internally tangent to the large circle, centered at the branch value w, that is the projection of z. We call this situation *shifted branching*.

With our generalized notion of branched circle packing, we can now identify the precise location of each branch value, and branch values need not be the images of the center of any of the circles in the packing. That is to say, although it is a discretization, the packing precisely determines a branched covering map from the carrier to the ambient space.

Given a classical finite Blaschke product $f : \mathbb{D} \to \mathbb{D}$, and a finite combinatorial disc K, we may now ask whether there exists a packing of K with generalized branching that lives on the Riemann surface of f and whose boundary discs are tangent to the boundary of the surface, so that they project to horocycles in $\mathbb{D}$. If so, is this discrete Blaschke product unique up to normalization, for example if we fix the positions of two adjacent boundary circles? In particular, can we make a discrete finite Blaschke product $\tilde{\mathbf{b}}$ with generalized branching that lies on the Riemann surface of the classical degree 3 Blaschke product $\mathbf{B}$ discussed earlier? We are asking whether the extra real degrees of freedom afforded by shifted and singular branching allow us to make the branch values lie exactly at p_1 and p_2.

We do not yet have a complete answer to these questions. However, we can get close, using the *metric packing theorem* of Oded Schramm [12]. This remarkable topological theorem concerns representations of finite triangulations of the sphere by packings of closed metric balls with respect to an arbitrary Riemannian metric on the sphere. The packing exists and is unique once three mutually tangent balls have been specified to represent three given vertices belonging to one face of the triangulation. Note that in this generality the balls do not even have to be topological discs, but can be multiply connected!

Here is an approach to our question using Schramm's theorem. Given a finite Blaschke product $f : \mathbb{D} \to \mathbb{D}$, of degree d, say, there exists a unique polynomial p of degree d such that f and p have the same finite branch values and monodromy. Let S be the Riemann surface of p. In this case, S and U are both copies of the Riemann sphere and p represents the branched covering projection from S onto U. Let $\hat{K}$ be the triangulation of the sphere obtained by adding one extra vertex, labelled v_∞, to K, making it adjacent

to all of the boundary vertices of K. Our goal is to find a packing of $\hat{K}$ on S, such that the disc representing v_∞ is the preimage in S of the complement of the open unit disc. Thus v_∞ will be a branch vertex of valence d. Restricting the packing to the Riemann surface of f will then yield a discrete Blaschke product with the same branch values and monodromy as f.

For normalization, we choose two adjacent neighbors of v_∞, and choose mutually tangent discs to represent them on S. These last two prescribed discs should contain no branch points. We would like to apply Schramm's metric packing theorem using the pullback metric on S whose length element is given by $|p'(z)|\,|dz|/(1+|p(z)|^2)$. This is the pullback of the spherical metric by p. But there is a difficulty: this infinitesimal metric vanishes at the branch points of p, including ∞, so it does not define a Riemannian metric.

To proceed, we *mollify* the pullback metric in the neighbourhood of each singularity by adding the spherical metric element multiplied by a smooth circularly symmetric bump function supported in a small disc around the singularity. In this way we can produce a sequence of Riemannian metrics that converges to the pullback metric. For each metric in the sequence, the three prescribed circles are the boundaries of metric balls. So we can apply Schramm's theorem to each metric in this sequence, to obtain a sequence of packings of $\hat{K}$, all with the same boundary normalization given by our three prescribed discs (which remain balls in the mollified metrics). Now we extract a convergent subsequence of these packings. The limit packing will respect all the required tangency conditions and will be a packing of closed metric balls in the pullback metric. So why are we not finished? The issue is that some of these balls could have radius zero in the limit. As we approach the limit, parts of the packing may degenerate, being sucked into singular branch points. Whether or not this happens depends in a complicated way on K and f and the choice of normalization. For a reasonable existence and uniqueness theorem, it seems that packings in which some vertices are represented by single points have to be allowed. We do not yet have a uniqueness proof, perhaps because we lack a stability version of the uniqueness statement in Schramm's theorem.

In any case, Schramm's theorem is not constructive, in the sense that it does not come with an algorithm to approximate numerically the packings whose existence it guarantees. Do we have any hope of *computing* packings with generalized branching, in the way that we can compute packings with traditional branching? The answer is yes, and how to do this will be the focus of the next two sections. The price we pay is that we will not get to specify in advance the covering surface that the packing lies on. Instead we get to specify where the branching lies with respect to the triangulation. By way of analogy, it is easy to write down a polynomial with given branch

points, but it is a much harder computational problem to find a polynomial with given branch values and monodromy.

Mimicking the individual classical Blaschke product **B** exactly may seem to be a lot of effort for little gain. However, if one thinks more broadly of the family of degree 3 Blaschke products parameterized continuously by the points p_1 and p_2, the goal of continuously parameterized discrete versions makes more sense. It also makes more sense when the very existence of the discrete versions depends on this added flexibility, as with our broken Ahlfors example. Let us now describe the mechanics.

5. Local Mechanics

We will describe local combinatorial modifications that coerce the standard iterative circle packing algorithm into producing the two forms of discrete generalized branching that correspond to a simple branch point. Recall that these are *singular* and *shifted* branching. For each type of branching, we first identify a *black hole* H, which is a small combinatorial locale to support the branching, and its *event horizon* $\Gamma = \partial H$, the chain of surrounding edges. Outside of the event horizon, our circle packing mappings are defined in the usual way, so that in an annulus about the black hole one may observe the typical topological behavior described earlier. Adjustments hidden inside the black hole, however, incorporate extra vertices and edges which do not correspond to vertices and edges of the original triangulation. Some of these new vertices represent *guide circles* which overlap with their neighbors. The overlap angle parameters provide the two real degrees of freedom needed to move the branch point around.

5.1. **Background.** We have recalled some circle packing mechanics, but as our work involves new features, we review the basics.

A complex K is assumed to be given. The fundamental building blocks of K are its *triangles* and *flowers*. The triangles are the faces $\langle v, u, w\rangle$. The flowers are sets $\{v; v_1, v_2, \cdots, v_{n+1}\}$ where v is a vertex and $v_1, \cdots, v_{n+1}$ is the counterclockwise list of neighbors in K. These neighbors, the *petals*, define the fan of faces containing v. Here n is the number of faces, so when v is interior, then $v_{n+1} = v_1$.

In talking about a circle packing P for K, the radii and centers are, of course, the ultimate target. However, proofs of existence and uniqueness (and computations) depend on the standard Perron methods first deployed in [4]. Given K, the fundamental data lies in three lists: the *label* $R = \{R(v) : v \in K\}$, edge overlaps $\Phi = \{\Phi(e) : e = \langle u, v\rangle\}$, and target angle sums $A = \{A(v) : v \in K\}$. Each will require some extension.

- **Labels:** The labels $R(v)$ are putative radii (they become actual radii only when a concrete packing is realized).

- **Overlap Angles:** For an edge $e = \langle v, w \rangle$ of K, the overlap $\Phi(e)$ represents the desired (external) angle between the circles c_v, c_w in P. Interest is often in "tangency" packings; in this case, Φ is identically zero and hence does not appear explicitly. However, from Thurston's first introduction of circle packing, non-tangency packings were included and we need them here.
- **Target Angle Sums:** Given R and Φ, one can readily compute for any triangle $\langle u, v, w \rangle$ the angle which would be realized at v if a triple of circles with the given labels (as radii) and edge overlaps were to be laid out. The *angle sum* $\theta_{R,\Phi}(v)$ is the sum of such angles for all faces containing v. The target angle sum, $A(v)$ is the intended value for $\theta_{R,\Phi}(v)$. It is typically prescribed only when v is interior, and then must be an integral multiple of 2π, $A(v) = 2\pi k$; this is precisely the result when petal circles $c_{v_1}, c_{v_2}, \cdots, c_{v_n}$ wrap $\frac{A(v)}{2\pi} = k$ times about c_v.

A circle packing for K is computed by finding a label R, termed a *packing label*, with the property that $\theta_{R,\Phi}(v) = A(v)$ for every interior vertex v. Typically, the values $R(w)$ for boundary vertices w are prescribed in advance. With label in hand, one can position the circles in the pattern of K to get P. This positioning stage is a layout process analogous to analytic continuation for analytic functions. Only after the layout does one finally realize circle centers. Our work will be carried out in hyperbolic geometry, where we use the fact that boundary radii may be infinite when associated with horocycles. The various existence, uniqueness, and monotonicity results needed for our applications would hold in euclidean geometry as well.

The Perron method for computing a packing label proceeds *via superpacking* labels, that is, labels R for which the inequality $\theta_{R,\Phi}(v) \leq A(v)$ holds for all interior v and which has values no less than the designated values at boundary vertices. It is easy to show that the family of superpacking labels is nonempty and that the packing label is the family's infimum. This infimum may be approximated to any desired accuracy by an iterative adjustment process — this is basically how `CirclePack` computations are carried out. The following condition $(\star)$ is required to ensure non-degeneracy: If $\{e_1, e_2, \cdots, e_k\}$ is a simple closed edge path in K which separates some edge-connected non-empty set E of vertices from ∂K, then the following inequality must hold

$$(\star) \qquad \sum_{1}^{k} (\pi - \Phi(e_j)) \geq 2\pi + \sum_{v \in E} (A(v) - 2\pi).$$

Our work here requires the following extensions to the given data:

- **Zero Labels:** We will introduce situations in which labels for certain interior vertices go to zero, corresponding with circles that in

the final configuration have degenerated to points, namely to their centers. Zero radii actually fit quite naturally into the trigonometric computations, but we will only encounter them for isolated vertices.

- **Deep Overlaps:** When introducing circle packing, Thurston included specified overlaps $\Phi(e)$, as we do. In general, however, the restriction $\Phi(e) \in [0, \pi/2]$ is required for existence. We will allow *deep overlaps*, that is overlaps in $(\pi/2, \pi]$. Note that overlaps may already be specified as part of the original packing problem under consideration, but these will remain in the range $[0, \pi/2]$. It is only in the modifications within black holes that deep overlaps may be needed, and these will carry clear restrictions.
- **Branching:** Traditional branching, described earlier in the paper, is associated with target angle sums $A(v) = 2\pi k$ for $k \geq 2$. These are subject to the condition $(\star)$ noted above, which concerns interactions of combinatorics and angle sum prescriptions. It traces to the simple observation that it takes at least 5 petal circles to go twice around a circle. The tight conditions emerged first in work on branched tangency packings in [8] and [5]. These were modified to incorporate overlaps in [6]; Condition $(\star)$ parallels the conditions there while allowing equality, which is associated with zero labels in black holes, as we see shortly.

The monotonicities behind the Perron arguments depend on our ability to realize any face $\langle u, v, w\rangle$ with a triple of circles $\{c_v, c_u, c_w\}$ having prescribed radii and overlaps. To include deep overlaps and zero labels, it is relatively easy to see that some side conditions on Φ are required. What we need is given in the following lemma, a minor extension of the hyperbolic results in [3].

Lemma 1. *Given three hyperbolic radii, r_1, r_2, r_3, at least two of which are non-zero, and given three edge overlaps $\phi_{12}, \phi_{23}, \phi_{31} \in [0, \pi]$ satisfying $\phi_{12} + \phi_{23} + \phi_{31} \leq \pi$, there exists a triple $\langle c_1, c_2, c_3\rangle$ of circles in $\mathbb{D}$ which realize the given radii and overlaps.*

The angles α, β, γ of the triangle T formed by their centers are continuous functions of the radii and overlaps and are unique up to orientation and conformal automorphisms of $\mathbb{D}$. Moreover α is strictly decreasing in r_1, while area(T) is strictly increasing in r_1. Likewise, β (resp. γ) is strictly increasing in r_1 (assuming r_2 (resp. r_3) is finite).

In our generalized branching, zero labels and deep overlaps are temporary devices only within black holes; we modify the combinatorics and set overlap parameters in there to control apparent branch locations. The results, however, are then used to layout a circle packing P for the original complex K; P itself does not involve any zero labels or deep overlaps, and aside from

ambiguity about one circle in the shifted branching case, P is a normal circle packing configuration.

We conclude these preparations by noting the two conditions which are necessary to guarantee existence and uniqueness of the packings. Namely, condition ($\star$) and this condition ($\star\star$)

($\star\star$) $\quad \Phi(e_1) + \Phi(e_2) + \Phi(e_3) \leq \pi$ if edges $\{e_1, e_2, e_3\}$ form a face of K.

With this, we may now describe our two discrete generalized branching mechanisms.

5.2. **Singular Branching.** Singular branching is used to simulate a branch point lying in an interstice of P_K. The interstice is defined by a face $\langle v_1, v_2, v_3 \rangle$, corresponding to red, green, and blue circles, respectively, in our illustrations. The black hole is the union of the target interstice and the three interstices sharing its edges. The combinatorics imposed and the event horizon are illustrated in Figure 6. The complex K, modified inside the black hole, will be denoted $\widetilde{K}$ and serves as our complex for subsequent computations. The circles of Figure 6 are a device for display only and are not part of the final circle configuration. Indeed, before computing the circles of the branched packing we need to prescribe target angle sums, A, and edge overlaps, Φ.

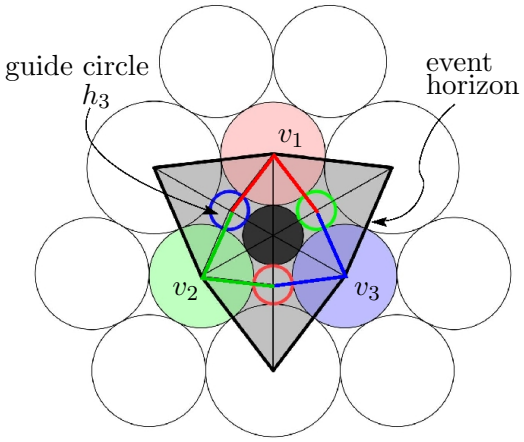

FIGURE 6. Combinatorics for a singular black hole.

Interior to the event horizon we have introduced 4 additional vertices. Three of these, h_1, h_2, h_3, are termed *guide circles* since they help guide the circles for v_1, v_2, and v_3; we label h_3 in Figure 6. A fourth vertex g, in the center, is called the *vanishing circle*. Specify target angle sums $A(v) \equiv 2\pi$ for all interior vertices $v \in \widetilde{K}$ with the exception of g, setting $A(g) = 4\pi$.

Singular branching is controlled *via* overlap parameters associated with a partition of π, $\gamma_1 + \gamma_2 + \gamma_3 = \pi$. For $i = 1, 2, 3$, the value $\gamma_i > 0$ represents

the overlap angle prescribed in Φ for the edges from v_i to the guide circles on either side. These three pairs of edges are color coded in Figure 6. We set $\Phi(e) = 0$ for all other edges of $\widetilde{K}$.

Before describing how these parameters are chosen, observe that we are assured of a circle packing $\widetilde{P}$ for $\widetilde{K}$ with label $\widetilde{R}$, interior angle sums A, and overlaps Φ. In particular, if Γ denotes the chain of 6 colored faces surrounding the vanishing circle, g, then condition $(\star)$ holds whenever the angle sum prescription $A(g)$ satisfies $A(g) \leq 4\pi$, with equality when $A(g) = 4\pi$. Traditional Perron and layout arguments imply the existence and uniqueness of the circle packing $\widetilde{P}$ in which the circle for g has radius zero. An example of the result is illustrated in Figure 7. For this we set roughly $\gamma_1 = 0.22\pi, \gamma_2 = 0.40\pi$, and $\gamma_3 = 0.37\pi$.

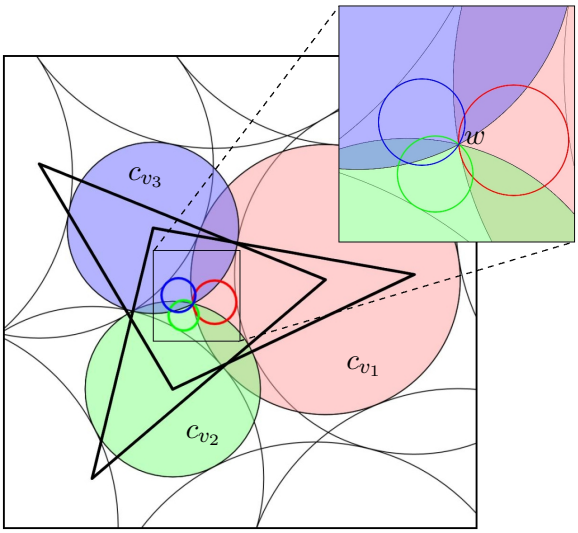

FIGURE 7. Image circle packing in the neighborhood of singular branching, and detail zoom.

This image takes some time to understand. The circle for g has degenerated to a point, the branch value, which is at the common intersection point of the circles for v_1, v_2, v_3 and also for guide circles h_1, h_2, h_3; it is labeled w in the detail zoom. The branching is confirmed in the larger image by observing how the event horizon wraps twice about the branch value. If we disregard the guide circles and the vanishing circle, the remaining circles of $\widetilde{P}$ realize a tangency circle packing for the original complex K. That is, the black hole structure was needed only to guide the layout of the original circles.

This portion of the layout illustrates singular branching as we described it in Section 4: the circles lie on a locally two-sheeted surface S branched above w. Note, for instance, that the overlap of the red and blue circles

is only in their projections to the plane: in actuality, the red part of the intersection is on one sheet of S and the blue is on the other. This shows in the orientation of the red, green, blue, which in projection is the reverse of their orientation in P_K.

Finally, what about choosing parameters $\gamma_1, \gamma_2, \gamma_3$ to get the desired branch point? Figure 8 illustrates our scheme. We have isolated the interstice formed by circles for v_1, v_2, v_3 in P_K. The dashed circle is the common orthogonal circle through the intersection points and defines a disc D which will be treated as a model of the hyperbolic plane. Point p indicates a location where one might wish to have branching occur. Hyperbolic geodesics connecting p to the three intersection points on ∂D determine angles $\alpha_1, \alpha_2, \alpha_3$, indexed to correspond with the vertices v_1, v_2, v_3. We then define $\gamma_j = \pi - \alpha_j, j = 1, 2, 3$. One has complete freedom to choose γ_1 and γ_2 in this scheme, subject to conditions $\gamma_1, \gamma_2 > 0$ and $\gamma_1 + \gamma_2 < \pi$. We will be seeing examples for p and the other three red branch points later, in Figure 13.

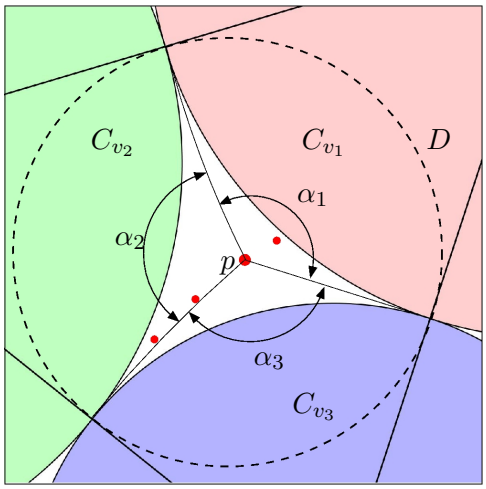

FIGURE 8. The parameter scheme for singular branching.

5.3. **Shifted Branching.** Shifted branching simulates a branch point lying within an interior circle of P_K. Of course, when that point is the center, then traditional branching would be the easy choice. This will be incorporated naturally in our parameterized version, however, so we need not separate out this case.

Suppose v is the interior vertex whose circle is to contain the shifted branch point. The black hole combinatorics shown in Figure 9 are imposed on the flower for v. (Note that once again, the circles here are used for display but are not part of our target packing.)

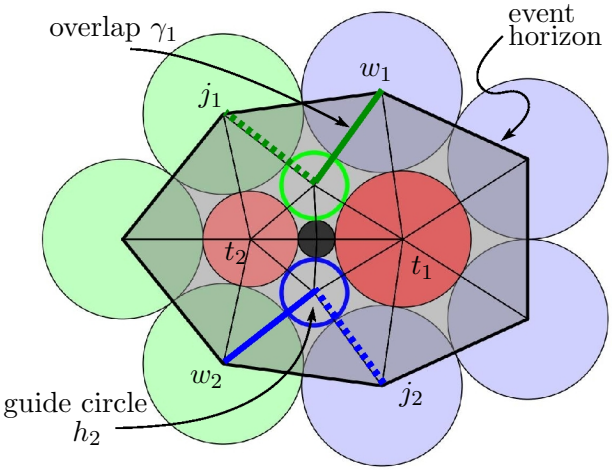

FIGURE 9. Combinatorics for a shifted black hole.

The event horizon is the chain of edges through the original petals of the flower for v (seven petals, in this case, green and blue). Interior to this horizon, we split v, replacing it with the twin vertices, denoted t_1 and t_2 and corresponding to the circles in two shades of red. We introduce two guide circle vertices h_1, h_2, respectively green and blue, and a vanishing circle vertex g, black; we label only guide circle h_2 in the figure. With these combinatorics inside the event horizon, we again have a new complex $\widetilde{K}$, for which we need target angle sums A and edge overlaps Φ.

Each guide circle neighbors two original petals, denoted w_i and j_i. The petal j_i is known as the *jump* circle because its guide circle h_j and an associated parameter γ_i facilitate its detachment from one twin and its attachment to the other. The parameters here are γ_1 and γ_2, chosen independently within $[0, \pi]$, and used to define overlaps with the guide circles. In particular, for $i = 1, 2$, prescribe $\Phi(\langle h_i, w_i \rangle) = \gamma_i$ and $\Phi(\langle h_i, j_i \rangle) = \pi - \gamma_i$; the edges are shown as solid and dashed lines, respectively, in Figure 9. The other overlaps in Φ are zero, so Condition $(\star\star)$ holds. Target angle sums are defined as before, namely, $A = 2\pi$ at interior vertices of $\widetilde{K}$, save for the vanishing circle, with $A(g) = 4\pi$.

Putting aside the choice of jump circles and parameters for now, we are assured of a circle packing $\widetilde{P}$ for $\widetilde{K}$ with label $\widetilde{R}$, interior angle sums A, and overlaps Φ. If Γ is the chain of edges through the four neighbors of g, edges for which tangency is specified, then equality holds in condition $(\star)$, so in $\widetilde{R}$ the radius of the vanishing circle is necessarily zero.

Figure 10 illustrates the circle packing for $\widetilde{K}$ before we prescribe the branching, in other words, with the target angle sum at g kept at 2π. We abuse notation by referring to circles by their vertex indices. The original petal circles, starting with j_1 and ending at w_2, are shown in green: these

are tangent to twin t_2. Likewise, those starting at j_2 and ending at w_1 are shown in blue: these are tangent to twin t_1.

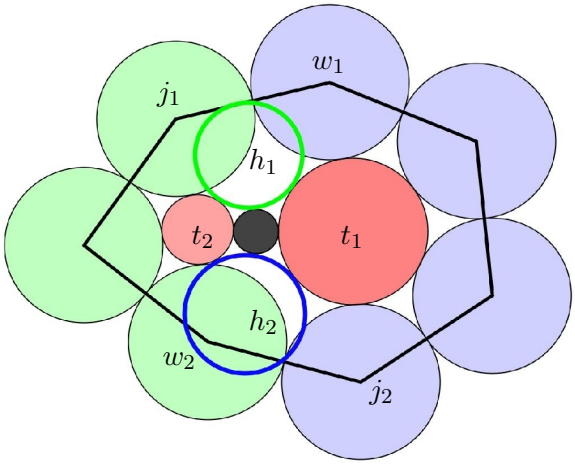

FIGURE 10. The jump circles and parameters are set for a shifted black hole before the branching is imposed.

We consider the action at guide circle h_1. First, recall two facts: (1) When a triple of circles has edge overlaps summing to π, then the three share a common intersection point; and (2) when circles overlap by π then one is interior to the other. Here is how the machinery works at h_1. The circle for w_1 is tangent to twin t_1, j_1 is tangent to twin t_2, while h_1 is tangent to both twins. When $\gamma_1 = 0$, the overlap of π between h_1 and j_1 forces the jump circle j_1 to be tangent to t_1. As γ_1 increases, however, the jump circle separates from t_1 until, when γ_1 reaches π, w_1 has been pulled in to be tangent to t_2. In other words, γ_1 acts like a dial: when positive, it detaches the jump circle from t_1, and as it increases, it moves the jump further around t_2. The mechanism is similar for guide circle h_2, as γ_2 serves to detach the jump circle j_2 from t_2 and move it further around t_1.

Typical parameters $\gamma_1 = 0.7\pi$ and $\gamma_2 = 0.4\pi$ were specified for Figure 11. Maintaining these while adding branching at g, i.e., setting $A(g) = 4\pi$, gives the configuration of Figure 11. As usual with branching, the image is rather difficult to interpret, so we point out the key features: The twin circles and guide circles are all tangent to g, and the radius for g is zero, so these four circles meet at a single point. The twin circles (red) are nested, as are the guide circles (green and blue). The branch value is the white dot in the detail zoom, at the center of the small twin circle and labeled w; we explain this shortly. To confirm the topological behavior of generalized branching, note that the circles for the original petals of v wrap twice around w — just follow the image of the event horizon in the larger image as it goes through the petal centers and tangency points. The petals are green and blue in the

larger image, corresponding, as in Figure 10, to which twin they are tangent to. The jump circles j_1, j_2 are also labeled.

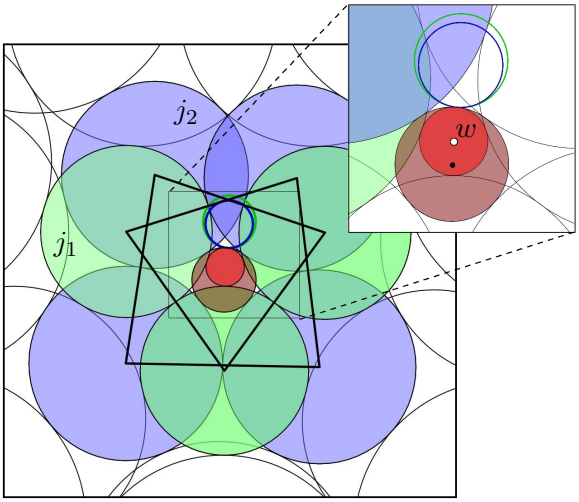

FIGURE 11. Image circle packing in the neighborhood of shifted branching, with detail zoom.

As with the singular branch image, the configuration of Figure 11 first our description in Section 4: on treats the image as the projection of circles lying on a two-sheeted surface S branched over w. To see this, consider the twins in the detail zoom: t_1 is the larger twin, with center at the black dot and radius r_1. The smaller twin has center at w and radius $r_2 < r_1$. Now imagine attaching a string of length r_1 at the black dot and using it to draw the circle for t_1 on S. As the string sweeps around, it will snag on the white dot at w and, like a yo-yo, trace out the smaller twin on S before finishing t_1. In other words, the union of the two twin circles together is the projection of all points on S which are distance r_1 from the center of t_1 (that is, distance *within* S). Exactly this thought experiment was the genesis of shifted branching.

If we disregard the guide circle circles and twins, the remaining circles constitute a traditional tangency circle packing P for K, with the caveat that generically the circle for v is ambiguous — neither the circle for t_1 nor for t_2 alone can serve as c_v. We need to live with this ambiguity to achieve the branching behavior we want outside the event horizon. (Having said this, there are (many) settings which lead to identical twin circles, so P then has this common circle as c_v. All these configurations are identical and are nothing but the circle packing we get when we choose traditional branching at v.)

This brings us to the matter of configuring black hole combinatorics and parameters for this shifted branching; that is, choosing the jump circles j_1, j_2 and their associated overlap parameters γ_1, γ_2. We describe our scheme by referring to Figure 12, which is the flower for C_v in P_K.

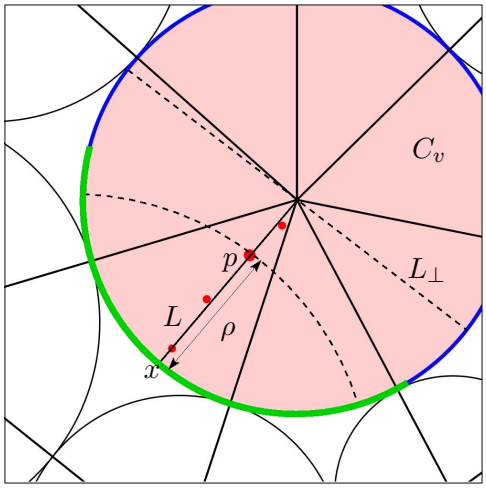

FIGURE 12. Choosing jumps and overlap parameters for shifted branching.

The ultimate goal is to simulate branching at some point within C_v, such as the indicated point p. In mapping to the branched image packing P, the image of the boundary of C_v wraps continuously around the boundaries of both twin circles (as we described earlier in referring to the branched surface S). The jump circles and parameters serve to split the boundary of C_v into two arcs, the blue one will be carried to t_1, the green, to t_2.

Here we need to observe how the jump and its parameter work together. Recall that in the image packing, $\gamma_1 \in [0, \pi]$ acts like a dial: The value $\gamma_1 = 0$ forces j_1 to be tangent to both twins. As γ_1 increases, it pushes j_1 away from t_1 and further onto t_2. When γ_1 reaches π, it forces the counterclockwise petal w_1 to become tangent to t_2. This is a transition point — at this juncture, we could designate w_1 as the jump circle and reset γ_1 to 0 without altering anything in the image packing. By then increasing the new γ_1 with the new jump circle, we could push yet more boundary onto t_2. In summary, then, our circle packing map pushes more of C_v onto t_2 by increasing γ_1 and/or moving the designated jump j_1 clockwise. Likewise, on the other side it pushes more of C_v onto t_2 by decreasing γ_2 and/or moving the designated jump j_2 counterclockwise.

To illustrate with the point p of Figure 12, the scheme uses the various labeled quantities: The point x where the radial line L from the center of

C_v through p hits C_v; the distance ρ from p to x; the circular arc (dashed) through p and orthogonal to C_v; and the diameter $L_\perp$ perpendicular to L.

To inform our choice of jumps and parameters, we take inspiration from the properties of the branch value w in the eventual image packing — that is, the center of the smaller twin, t_2. In qualitative terms, the blue arc of C_v should map to t_2, the rest of C_v to t_1. The point x should map to the point of t_2 antipodal to the tangency point of t_1 and t_2. The ratio of ρ to the radius of C_v should reflect the ratio of the radii of the two twins. Thus, when p moves close to C_v, twin t_2 gets smaller, while as p approaches the center of C_v, the radius of t_1 approaches that of t_2. There is no way to ensure these outcomes precisely — one cannot know, *a priori*, the outcomes in the image packing, as all the circles get new sizes during computation. We will not burden the reader with the messy details, but we have implemented methods which realize these qualitative behaviors. We illustrate for p and the other three red branch points later, Figure 14.

6. Fixing an Ahlfors Function

After successfully constructing a discrete Ahlfors function $\mathbf{w}$ for a combinatorial annulus K in §2.2, we showed in §3 how easily that construction can fail. Making small modifications to K that broke its translational symmetry, we obtained a new combinatorial annulus K' which does not support a discrete Ahlfors function. The problem is non-trivial holonomy, and we illustrated in Figure 5 with an attempt at traditional branching using the same midline vertices v_1, v_2 we had used for $\mathbf{w}$.

It seems clear that for K' the missing translational symmetry can be blamed for the failure. We now apply the flexibility of generalized branching to repair the damage. Since K' still has a midline and reflective symmetry across it, we adopt the following strategy: proceed with traditional branching at vertex v_1, but use shifted branching near v_2. Symmetry simplifies our search for the correct branching parameters in the black hole for v_2: namely, if we choose vertex j_1 to be symmetric with w_2 across the midline, and likewise, j_2 symmetric with w_1, and if we specify $\gamma_2{=}\pi - \gamma_1$, then the shifted branch value must remain on the midline. After some experimental tinkering, one can in fact annihilate the holonomy and replicate the success we saw for the original complex K — the process works. We do not show the image packing P because it is essentially indistinguishable from Figure 4. The point is that we are able to make the red cross-cuts coincident.

Admittedly, the fix was (almost) in for this example: we depended on reflective symmetry to reduce the parameter search from a two- to a one-dimensional problem. Nonetheless, it demonstrates well the need and potential for generalized branching. We close by discussing the broader issues.

7. Parameter Space

This paper is a preliminary report on work in progress. We have focused on generalized branching at a single point p in the interior of P_K. The location of p is continuously parameterized — e.g, by its x and y coordinates. We have defined discrete generalized branching which seems to handle patches of this parameter space. Thus, when p lies in an interior interstice, singular branching involves two real parameters, γ_1, γ_2. When p lies in an interior circle, shifted branching involves jump circles and parameters, but in our description of the mechanics it is clear that this, too, is just two real parameters. The continuity of these parameterizations may be phrased in terms of the branched packing labels R restricted to vertices on and outside of the event horizon.

While a proof remains elusive, experiments strongly suggest that this continuity does hold. For example, Figure 13 displays the branched circle packings associated with branching at the four red dots in Figure 8, progressing from lower left to upper right (the third of these is the packing for the distinguished point p from Figure 8). The branch value is roughly at the center in each image. Subject to this and related normalizations, the radii and centers of P appear to be continuous in γ_1, γ_2.

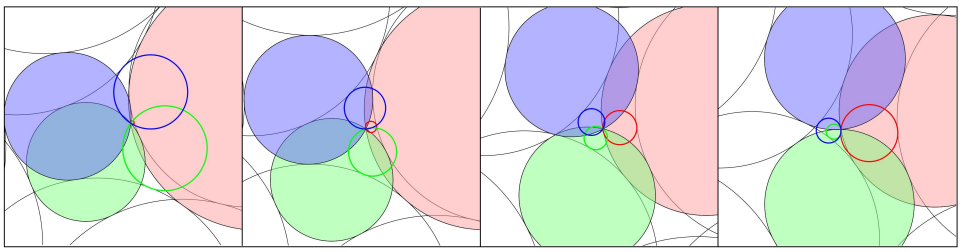

Figure 13. Singular branching for the four red branch points of Figure 8.

Figure 14 provides a similar sequence of shifted branched packings for the four red dots of Figure 8 (caution: the guide circles play different roles now). Again we have positioned the branch values roughly at the center in each image; the third one corresponds to Figure 11. Here, too, experiments suggest continuity in radii and centers as we manipulate the two shifted branching parameters.

Concatenating the 8 frames in these last two figures highlights another parameterization issue: How are our various patches of parameter space sewn together? If p lies on the mutual boundary of a circle and an interstice, for instance, its generalized branched packing may be treated as a limit of either singular branching from the interstice side or shifted branching from the circle side. We have *ad hoc* methods for such transitions, though we have

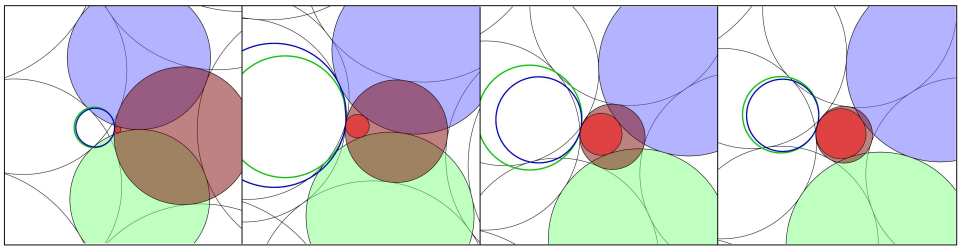

FIGURE 14. Shifted branching for the four red branch points of Figure 12.

yet to formalize the details of parameter alignment. Nevertheless, our images may give a feel for the transition: The interstice formed by $\{C_{v_1}, C_{v_2}, C_{v_3}\}$ in Figure 8 is contiguous to the circle C_v of Figure 12; that is, $v = v_1$. So the 8 frames from Figure 13 and Figure 14 together are part of a movie as the branch point transitions from singular to shifted. Image circles $\{c_{v_1}, c_{v_2}, c_{v_3}\}$ remain red, green, and blue, respectively, throughout these 8 frames. In the last frame from Figure 13 note that these three appear to be in clockwise order (as we discussed earlier). Compare this to the first frame of Figure 14: the red circle has now split into twins, with the branch value in the smaller twin, so the (small) red, green, and blue are again correctly oriented — the branch point has successfully punched though from the interstice to the circle, and in the last frame of Figure 14, it is nearing traditional branching at v. This is the type of experimental evidence supporting our contention that the two parameter patches can be aligned to maintain continuity.

8. Global Considerations

We stated in the introduction that our aim is to bridge the principal gap remaining in discrete function theory, namely the existence and uniqueness of discrete meromorphic functions. Although we have local machinery, we have not confronted the global problem head-on. A few words are in order.

Naturally, one of the first goals would be a more complete theory for discrete rational functions, branched mappings from $\mathbb{P}$ to itself. Here K would be a combinatorial sphere and one would need $2n$ branch points for a mapping of valence $n + 1$. Our hands-on approach still faces many hurdles in practice. On the sphere, for instance, there is no packing algorithm — Perron methods rely on the monotonicity of Lemma 1, which fails in the positive curvature setting. And in the setting of the discrete Ahlfors function, we depended on a symmetry of the complex K to reduce the search for correct overlap parameters to a one-dimensional problem. Though we believe generalized branching provides the flexibility to overcome the holonomy obstructions for a general complex, early attempts have faltered due to the curse of

(even small) dimension: we don't yet know how to search a two-dimensional space for parameters that will annihilate non-trivial holonomies.

We face other global difficulties as well. We list a few. We have restricted attention to *simple* branching; at least in the case of shifted branching, one can see a chance to allow higher order branching — replacing twins with triplets, etc. In general, one also needs to allow branching at more than one point, but the existence of branched packings then encounters global combinatorial issues. The notion of black holes will also need to be extended, since combinatorics may lead to patches of degenerate radii (versus isolated degenerate radii) for branch points in certain combinatorial environments.

In other words, there is considerable work to be done. Nevertheless, we contend that discrete generalized branching addresses — in theory if not in practice — the key obstruction remaining in discrete analytic function theory. This obstruction, of course, is not the only one — so get to work, David!

References

1. E. M. Andreev, *Convex polyhedra in Lobacevskii space*, Math. USSR Sbornik **10** (1970), 413–440 (English).
2. ———, *Convex polyhedra of finite volume in Lobacevskii space*, Math. USSR Sbornik **12** (1970), 255–259 (English).
3. James R. Ashe, *Generalized branching in circle packing*, Ph.D. thesis, Univ. of Tennessee, 2012, (advisor: Ken Stephenson).
4. Alan F. Beardon and Kenneth Stephenson, *The Schwarz-Pick lemma for circle packings*, Ill. J. Math. **35** (1991), 577–606.
5. Philip L. Bowers, *The upper Perron method for labelled complexes with applications to circle packings*, Proc. Camb. Phil. Soc. **114** (1993), 321–345.
6. Philip L. Bowers and Kenneth Stephenson, *A branched Andreev-Thurston theorem for circle packings of the sphere*, Proc. London Math. Soc. (3) **73** (1996), 185–215.
7. Charles R. Collins and Kenneth Stephenson, *A circle packing algorithm*, Computational Geometry: Theory and Applications **25** (2003), 233–256.
8. Tomasz Dubejko, *Branched circle packings, discrete complex polynomials, and the approximation of analytic functions*, Ph.D. thesis, University of Tennessee (advisor: Ken Stephenson), 1993.
9. ———, *Branched circle packings and discrete Blaschke products*, Trans. Amer. Math. Soc. **347** (1995), no. 10, 4073–4103.
10. David Minda and Burt Rodin, *Circle packing and Riemann surfaces*, J. d'Analyse Math. **57** (1991), 221–249.
11. Burt Rodin and Dennis Sullivan, *The convergence of circle packings to the Riemann mapping*, J. Differential Geometry **26** (1987), 349–360.
12. Oded Schramm, *Existence and uniqueness of packings with specified combinatorics*, Israel J. Math. **73** (1991), 321–341.
13. Kenneth Stephenson, `CirclePack` *software*, (1992–), http://www.math.utk.edu/∼kens.
14. ———, *Introduction to circle packing: the theory of discrete analytic functions*, Camb. Univ. Press, New York, 2005, (ISBN 0-521-82356-0, QA640.7.S74).